Few-Mode Lensed Fibers

He Wen, Huiyuan Liu, Yuanhang Zhang, Jian Zhao, Pierre Sillard, *Member, IEEE, Member, OSA*, Rodrigo Amezcua Correa, and Guifang Li, *Fellow, IEEE, Fellow, OSA*

***Abstract*—Few-mode lensed fiber for focusing multiple spatial modes with minimal distortion are proposed and investigated numerically and experimentally, for the first time to the best of the authors' knowledge. Although the conventional hyperbolic lens profile works effectively for the fundamental mode, it introduces severe distortion for high-order radial modes. This distortion is due to destructive interference between out-of-phase lobes in the radial direction. To reduce this distortion, we modify the lens profile to avoid such destructive interference. Focused images with significantly reduced distortions were observed in our experiments.**

***Index Terms*—Fiber lenses, optical signal processing, space division multiplexing.**

I. Introduction

LENSED fibers having a microlens directly fabricated at one end of the fiber are important devices for coupling power from lasers to fibers [1]–[3] or from fibers to other waveguide devices, such as photodetectors, semiconductor optical amplifiers [4], and in other non-telecom applications [5], [6]. Compared to coupling using bulk lenses, lensed fibers are small, lightweight, and robust to environmental effects. Although lensed fibers are mature for single-mode applications, to the best of the authors' knowledge, there are very few reports on their use in few-mode fibers. As space-division multiplexing (SDM) is being considered as a possible solution to surpass the nonlinear Shannon limit for single-mode fibers (SMF) [7], [8], devices to support few-mode signal will become necessary. As such, few-mode lensed fibers (FMLF), which can focus the modes supported by the host few-mode fiber (FMF), could play an important role in simultaneously coupling multiple spatial modes directly from FMF to other devices [9]. In contrast to single-mode fiber and multimode lensed fiber [2], [10], FMLFs not only require high coupling efficiency but also low distortion of all modes. In contrast to the recently reported FMF GRIN lens for collimation [11], FMLFs can be used to couple power into waveguides with sizes smaller than the FMF itself. This requires that the focused images produced by FMLF to be smaller than the fiber modes themselves.

In this paper, we first derive the FMLF profiles using the ray tracing method. We then obtain the focused output field distributions using the finite-difference domain-time (FDTD) method. We find that the traditional hyperboloid lens profile introduces severe distortions for high-radial-order modes. These distortions are significantly reduced after a correction is introduced to the FMLF profile. Finally, we characterize experimentally the performance of such FMLF, demonstrating focusing and low distortions.

II. FMLF Profile Design

Fig. 1(a) shows a schematic of a FMLF with its rotationally symmetric profile described by $r(z)$, where z denotes axial distance from the apex of the lens to any point on the lens surface. We assume all rays are parallel to the optical axis propagating through the lens and arrive at an image plane to the right of the FMLF at a working distance of $z = L$. To avoid wavefront distortion, all rays should experience an equal light path from an equal-phase plane before the lens apex at $z = -d$ to the image plane. Moreover, the magnification, k, defined as the ratio between the ray height on the image plane to the ray height on the equal-phase plane should be the same for all rays, as shown in Fig. 1(a). These two requirements result in the lens profile given by:

$$\sqrt{(L-z)^2 + (1-k)^2 r^2(z)} + n(z+d) = L + nd = \text{constant}, \tag{1}$$

where n is the refractive index of the lensed fiber. The left hand side of Eq. (1) is the optical path length (OPL) of a ray propagating off the optical axis and the right hand side of Eq. (1) is the OPL of the ray propagating along the optical axis. Eq. (1) ensures the same OPLs for all possible rays.

We obtain the lens profile function, $r(z)$, by rearranging Eq. (1), yielding

$$\frac{(z-a)^2}{a^2} - \frac{r^2}{b^2} = 1 \tag{2}$$

a hyperboloid, where $a = L/(n+1)$ and $b = L\sqrt{(n-1)/(n+1)/(1-k)}$.

To focus the fiber modes, the magnification k should range from -1 to 1. By setting $k = 0$, Eq. (2) recovers the lens profile for SMFs [4]. In the next section, we will show that the magnification k greatly affects distortions for high-radial-order modes.

Manuscript received May 31, 2018; revised September 7, 2018; accepted October 15, 2018. Date of publication October 19, 2018; date of current version November 28, 2018. This work was supported in part by the Army Research Office under Contracts W911NF1710553 and W911NF1710500. *(Corresponding author: He Wen.)*

H. Wen, H. Liu, Y. Zhang, R. Amezcua Correa, and G. Li are with the CREOL, College of Optics & Photonics, University of Central Florida, Orlando, FL 32816 USA (e-mail: he-wen@creol.ucf.edu; huiyuan@knights.ucf.edu; yuanhangzhang@knights.ucf.edu; r.amezcua@creol.ucf.edu; li@creol.uc.edu).

J. Zhao is with the College of Precision Instrument and Opto-Electronic Engineering, Tianjin University, Tianjin 300072, China, and also with the University of Central Florida, Orlando, FL 32816 USA (e-mail: nankaizhao@gmail.com).

P. Sillard is with the Prysmian Group, Parc des Industries Artois Flandres, Douvrin 62138, France (e-mail: Pierre.SILLARD@prysmiangroup.com).

Color versions of one or more of the figures in this paper are available online at http://ieeexplore.ieee.org.

Digital Object Identifier 10.1109/JLT.2018.2877098

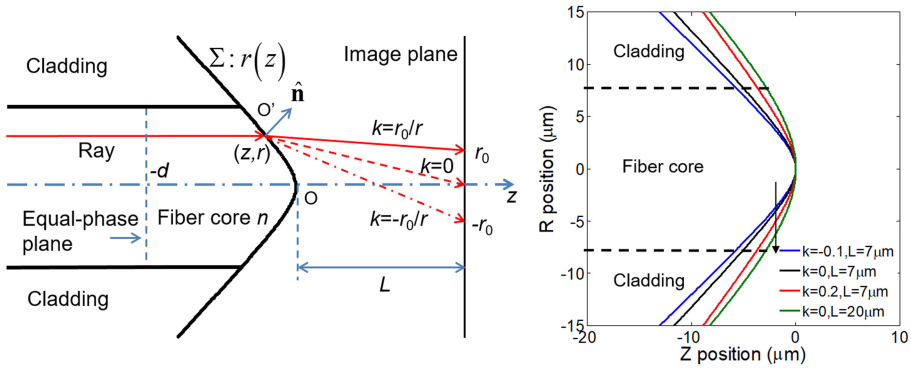

Fig. 1. (a) Geometry of the FMLF end face with ray tracing at the surface. (b) FMLF profiles with different parameters.

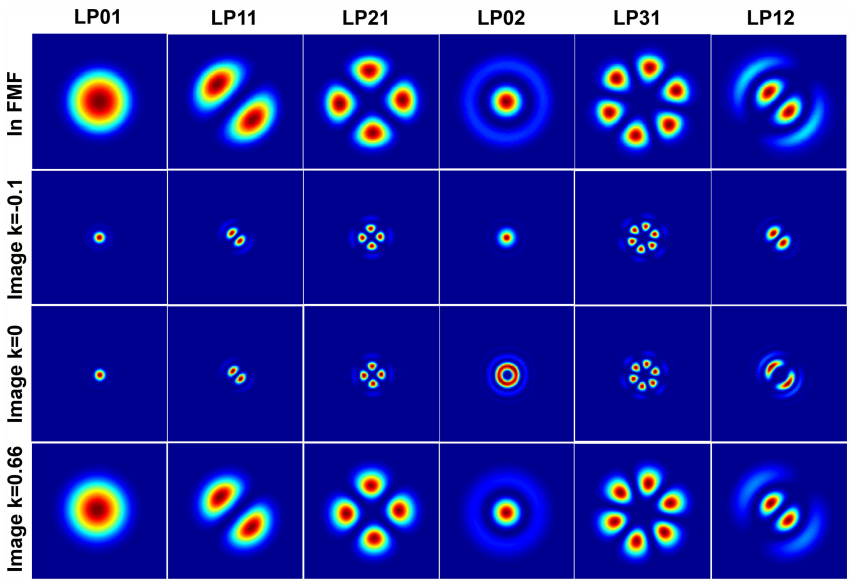

Fig. 2. Intensity profiles of the LP_{01}, LP_{11}, LP_{21}, LP_{02}, LP_{31} and LP_{12} modes in FMF (top) and images formed by a FMLF with k = −0.1, 0 and 0.66 (the 2nd to the 4th row). The area for all images is 24 × 24 μm^2.

Hyperboloidal profiles with different parameters are shown in Fig. 1(b). Generally, lenses with shorter working distances have sharper tips so as to strongly refract light. For the case of $k = 0$, all lenses have the same asymptotic cone half-apex angle: $\text{atan}(b/a) = \text{atan}[(n^2 - 1)^{1/2}] \approx 46.5°$ for silica fibers with the core refractive index of $n = 1.454$. This angle becomes larger (smaller) when k is a non-zero positive (negative) number. For negative k, in the ray tracing model, total internal reflection could occur for the incident rays at the lens/air interface when the incident angle becomes larger than the critical angle, which is asin $(1/n) \approx 43.5°$. This will increase the insertion loss of the lensed fiber and reduce the effective output aperture size. We determined the critical radius at which total internal reflection occurs is as follows:

$$r_c = \frac{L}{1-k}\sqrt{\frac{n-1}{n+1}\cdot\frac{1}{k\,(k-2)}}, \quad -1 < k < 0 \qquad (3)$$

Any ray incident outside of this critical radius is totally internally reflected. To reduce this effect, we increase the working distance L to ensure that the critical radius is larger than the core radius. To derive Eq. (3), we first calculated the slope of the tangent line of an arbitrary point on the lens surface and utilize the relation that the angle between the tangent line and the z axis is 90-degree larger than the incident angle. For a non-negative k, there is no total internal reflection.

III. Simulation

We simulated the performance of the proposed lensed fiber using a commercial FDTD package. The total simulation volume is divided into three regions, 1) the FMF, where linearly-polarized eigen-modes are excited, 2) the cone region, and 3) the free space propagation region from the lens surface to the image plane. The FMF refractive index and radius are 1.454 and 8 μm, respectively, for the core, and 1.44 and 62.5 μm for the cladding. The normalized V number is 6.5, therefore the FMF can support up to the LP_{12} mode. The intensity profiles of each mode inside the FMF are shown in the top row of Fig. 2.

The simulated output intensity profiles for each input fiber mode with $k = 0$ and a working distance of $L = 7$ μm are

displayed in the 3rd row. It is observed that the LP_{01}, LP_{11}, LP_{21}, LP_{31} modes are essentially undistorted at the image plane. The main lobes are de-magnified and without noticeable distortions. Some side lobes appear as a result of diffraction due to the limited aperture. Shorter working distances lead to stronger side lobes and a smaller gap between adjacent fringes.

The distortions of the LP_{02} and LP_{12} modes are, however, easily visible, especially for the main lobe at the center, where a dark spot at the origin has developed. These distortions can be attributed to the destructive interference between the main lobe and the out-of-phase first side lobe. The distortion of the LP_{12} mode is not as pronounced because it had a dark center prior to being focused by the FMLF. The reason for no distortion for the LP_{m1} modes is they have only one lobe in the radial direction. Multiple lobes in the azimuthal direction won't affect each other due to the rotational symmetry of the lens. These results indicate that the traditional single-mode lensed fiber design is not suitable for FMLF due to distortions for the LP_{mn} $(n > 1)$ modes, which contain multiple radial lobes with alternating phases.

An effective way to reduce distortions for the LP_{02} and LP_{21} modes is to prevent destructive interference between rays originating from two lobes with opposite phases by choosing $k \neq 0$ as shown in Fig. 1(a). The simulated output intensity profiles corresponding to each input fiber mode with $k = -0.1$ and 0.66 are shown in the 2nd and the 4th row of Fig. 2. It can be observed that the distortions for the LP_{02} and LP_{21} mode are effectively suppressed for these two values of k. Because of the sharper apex angle, the FMLF with $k = -0.1$ results in much tighter focused images compared with the FMLF with $k = 0.66$.

To clearly show the reduced distortions in the focused image for these two cases, we plot the radial intensity profiles of the LP_{01}, LP_{11}, LP_{02} and LP_{12} modes within the FMF (rescaled) and after they have been focused by the FMLF with $k = 0$ and -0.1 in Fig. 3. The dark center in LP_{02} completely disappears and the main lobe for $k = -0.1$ (red solid line) follows that of the rescaled LP_{02} mode (black dash-dotted line), in contrast to the case when $k = 0$ (blue dashed line) in Fig. 3(c). A similar improvement is observed for the LP_{12} mode in Fig. 3(d). These improvements are achieved at the expense of increased ripples outside the main lobes for the LP_{01} and LP_{11} modes and reduced side lobes for the LP_{02} and LP_{12} modes.

To evaluate the image quality quantitatively, we compute the coupling efficiency defined as the overlap integral between the focused field and the corresponding ideal LP mode with a proper scaling factor as follows:

$$CE = \max_{\alpha \in R^+} \left| \iint E_i(r)\, E_s^*(\alpha r)\, dr \right|^2 \tag{4}$$

where E_i and E_s are normalized fields of the images and original fiber modes, respectively and α is a rescaling factor.

Fig. 4 shows the coupling efficiencies for the LP_{01}, LP_{02} and LP_{12} modes as functions of the magnification k. It is clear that for negative k ranging from -0.1 to -0.3 or positive k ranging from 0.6 to 0.8, coupling efficiencies for the LP_{02} and LP_{12} modes improve substantially in comparison to the case where $k = 0$. Although negative k reduces the coupling efficiency for the LP_{01} mode in comparison with $k = 0$, maximum coupling

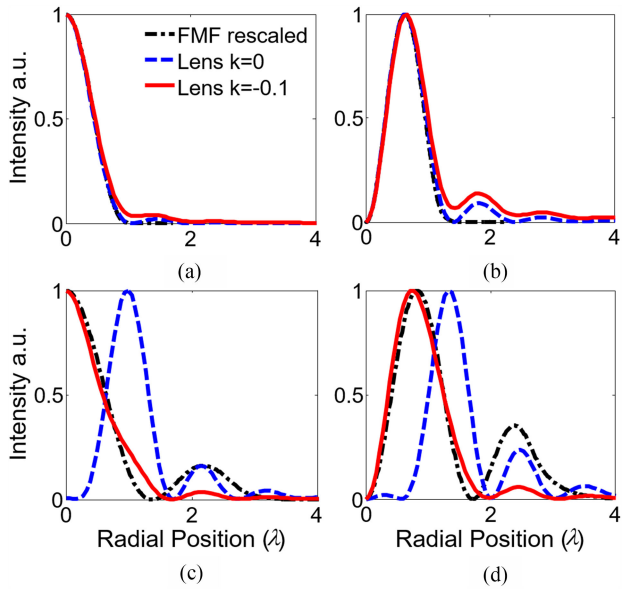

Fig. 3. (a)–(d) Radial intensity profiles of the LP_{01}, LP_{11}, LP_{02} and LP_{12} modes for the FMF (rescaled) and FMLFs with $k = 0$ and -0.1.

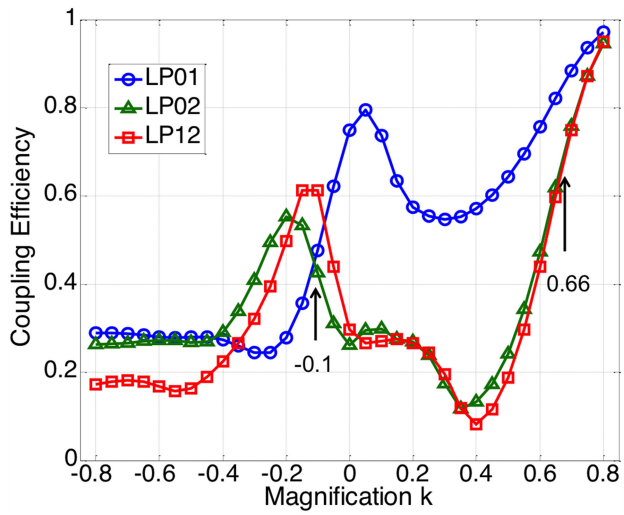

Fig. 4. Coupling efficiency of the LP_{01}, LP_{02} and LP_{12} modes using FMF lenses with different magnifications.

efficiencies for the LP_{02} and LP_{12} modes are achieved around $k = -0.1$, leading to tight focusing. In contrast, although large positive k increases the coupling efficiency for the LP_{01} mode in comparison with $k = 0$, maximum coupling efficiencies for the LP_{02} and LP_{12} modes are achieved at larger focused beam sizes. The choice of positive or negative magnifications depends on the degree of focusing required for particular applications.

Figure 5 shows the mode crosstalk matrix of the FMLFs with $k = -0.1$ and 0.66. Mode crosstalk is negligible for the FMLF with $k = 0.66$. However, relatively strong mode crosstalk exits between the LP_{01} and LP_{02} modes and between the LP_{11} and LP_{12} modes for the FMLF with $k = -0.1$. The reason for this difference is that modes of different orders are focused with different demagnifications when tightly focused ($k = -0.1$),

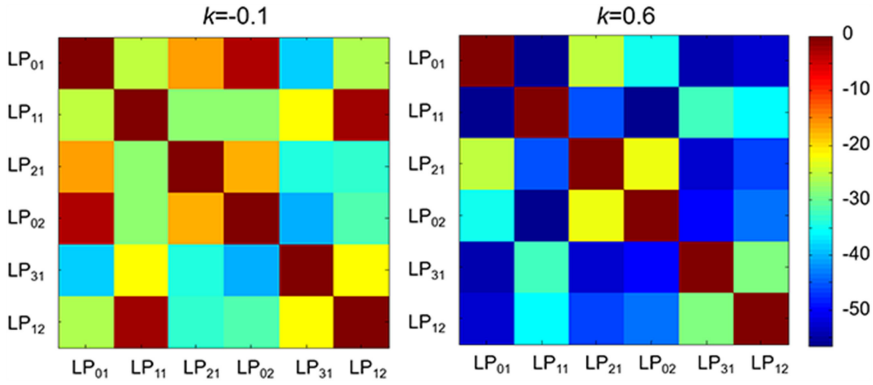

Fig. 5. Mode crosstalk matrix of the FMLFs with $k = -0.1$ (a) and $k = 0.66$ (b).

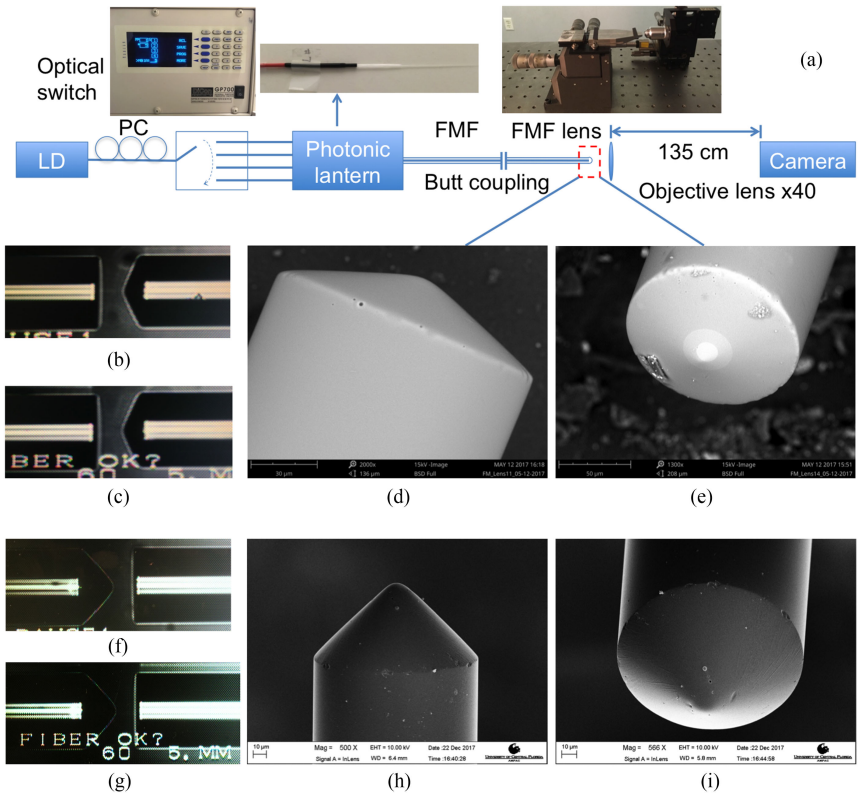

Fig. 6. (a) Experimental setup for FMLF test. LD: laser diode, PC: polarization controller. (b) and (c) Images taken by a fusion splicer from x and y directions and (d) and (e) SEM photos for the FMLF with a large apex angle; (f) and (g) optical images and (h) and (i) SEM photos of another FMLF with a small apex angle.

but nearly the same demagnification in loose focusing ($k = 0.66$). The difference in demagnifications between modes breaks the orthogonality between radial modes, but doesn't affect the orthogonality between azimuthal modes. Therefore, there is a trade-off between tight focusing and low crosstalk, which should be optimized for the application at hand.

IV. Experiment Verification

Figure 6 shows the experimental setup (a) used to characterize the FMLFs. In the setup, a mode-selective photonic lantern (PL) was used to excite the LP modes by selecting the appropriate input ports through an optical switch (Dicon GP700). The mode crosstalk of the PL itself is better than 10 dB. Since the PL is slightly polarization dependent, a polarization controller was used to optimize the intensity profiles for the FMF, as shown in Fig. 7(a)–(f). Butt coupling was used to couple the light output from the PL into the FMLF. A 40x objective lens mounted on a 3-axis stage was placed after the FMLF to project the output light onto a CCD camera (Electrophysics 7290A) at 1.35 meter away.

Two FMLFs with a working distance of 7 μm, but different apex angles were tested. The first one, with its optical and SEM images shown in Fig. 6(b), (c) and (d), (e), had an apex angle of

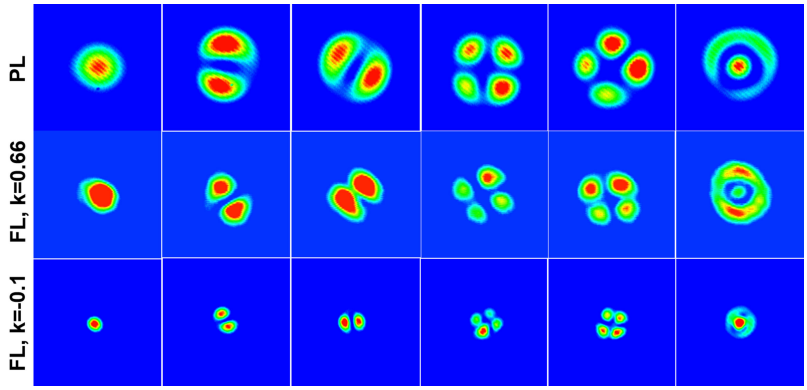

Fig. 7. Output intensity profiles of LP_{01}, LP_{11a}, LP_{11b}, LP_{21a}, LP_{21b} and LP_{02} modes from a photonic lantern in the top row, a FMLF with k = 0.66 in the middle row and a FMLF with k = –0.1 in the bottom row. The images are captured by a camera 1.35 meter away from a 40× objective lens.

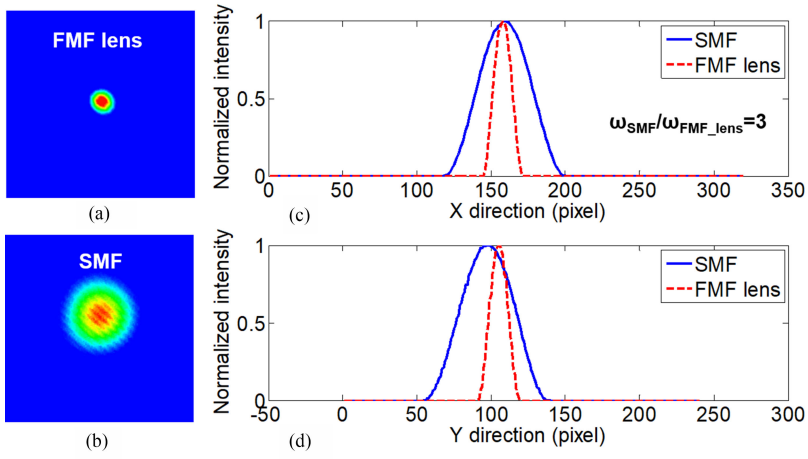

Fig. 8. Output LP01 mode size comparison between FMLF (a) and standard single mode fiber SMF28 (b). (c) and (d) Normalized intensity profiles averaged along y and x direction. The mode field diameter of the FMLF output is 1/3 of that of SMF28.

about 144 degrees, resulting in an approximate magnification of $k = 0.66$. The second one shown in Fig. 6(f)∼(i) had a sharper apex angle of about 92 degrees, producing a magnification of $k = -0.1$. The FMLFs were fabricated on a 6-LP- mode FMF with a numerical aperture of 0.13 [12] using plasma arc heating after polishing [13], [14]. In this approach, the apex angle is relatively easy to control, but accurate control of the profile is difficult. Here, the quality of the focused fundamental mode was used as a feedback mechanism to control the lens profile. The yield of this process is only about 33%.

The intensity profiles corresponding to all output modes were recorded and are shown in Fig. 7. All the output intensity profiles were measured at a fixed distance between the FMLF and the objective, indicating that the focal lengths were nearly identical for all modes. This allowed all the FMF modes to be coupled into other waveguides simultaneously. Compared with the output intensity profiles from the PL in the top row of Fig. 7, all modes were well focused by the FMLF with negligible distortions. As expected, the FMLF with a smaller apex angle, having stronger focusing ability, produces smaller images, as shown in the bottom row of Fig. 7 as compared to those in the middle row. Quantitatively, the LP_{01} mode field diameter was reduced to ∼2.7 μm, as shown in Fig. 8, in comparison with the 9-micron size of the fundamental mode of the SMF. The size was twice as large as the design value due to deviations from the designed lens profile. Other distortions include fabrication defects, such as geometric asymmetry, surface roughness, and pits and holes as seen in the SEM images in Fig. 6(h) and (i). Since the size of holes is less than 1 μm, shorter than wavelength, these holes mainly produce excess loss; effect on the output beam profiles is negligible. To further improve the quality of the focused beam, the fabrication accuracy of the lens profile must be improved using other approaches such as laser micromachining [15] or focused ion beam milling [16].

The measured insertion loss of the 1-m long FMLF with a smaller apex angle for the LP_{01}, $LP_{11a,b}$, $LP_{21a,b}$, and LP_{02} modes were 1.0, 2.3, 1.3, 1.0, 2.6 and 2.7 dB, respectively, in contrast to 0.4, 0.4, 0.5, 0.7, 0.7 and 0.5 dB for the FMLF with a larger apex angle. The larger insertion losses of the FMLFs with a smaller apex angle is likely due to stronger back reflection at the end facet at a large incident angle, as the critical radius for total internal reflection, evaluated by (3) for the designed FMLF ($L = 7$ μm, $k = -0.1$), is 6 microns, which is smaller than the core radius.

V. Conclusion

We propose and demonstrate FMLF used to couple light from FMFs to smaller waveguides. The traditional SMF lens design severely distorts the output intensity profiles for high-order radial modes. A new FMLF design is proposed that reduces distortion for all modes. The new design has been verified by numerical simulations and experiments. The performance and fabrication tolerance of the FMLF can be improved by incorporating a coreless fiber [17], [18] or a quarter pitch length of graded-index fiber with a lens profile [19] at the end.

Acknowledgment

He Wen would like to thank Dr. Shi Chen and Mr. Jian Zhao for their help in SEM imaging.

References

[1] J. John, T. S. M. Maclean, N. Ghafouri-Shiraz, and J. Niblett, "Matching of single-mode fibre to laser diode by microlenses at 1.5 μm wavelength," *Proc. IEE—Optoelectron.*, vol. 141, pp. 178–184, 1994.

[2] C. A. Edwards, H. M. Presby, and C. Dragone, "Ideal microlenses for laser to fiber coupling," *J. Lightw. Technol.*, vol. 11, no. 2, pp. 252–257, Feb. 1993.

[3] K. Kurata, K. Yamauchi, A. Kawatani, E. Tanaka, H. Honmou, and S. Ishikawa, "A surface mount single-mode laser module using passive alignment," *IEEE Trans. Compon., Packag., Manuf. Technol. B*, vol. 19, no. 3, pp. 524–531, Aug. 1996.

[4] R. A. Boudreau and J. S. LaCourse, "Packaging of semiconductor optical amplifiers," *Proc. SPIE*, vol. 1177, pp. 245–256, 1990.

[5] D. R. Rivera, C. M. Brown, D. G. Ouzounov, W. W. Webb, and C. Xu, "Use of a lensed fiber for a large-field-of-view, high-resolution, fiber-scanning microendoscope," *Opt. Lett.*, vol. 37, pp. 881–883, 2012.

[6] K. Taguchi, H. Ueno, T. Hiramatsu, and M. Ikeda, "Optical trapping of dielectric particle and biological cell using optical fibre," *Electron. Lett.*, vol. 33, pp. 413–414, 1997.

[7] A. Chralyvy, "Plenary paper: The coming capacity crunch," in *Proc. 2009 35th Eur. Conf. Opt. Commun.*, 2009, Paper 1.0.2.

[8] R. J. Essiambre and R. W. Tkach, "Capacity trends and limits of optical communication networks," *Proc. IEEE*, vol. 100, no. 5, pp. 1035–1055, May 2012.

[9] W. J. Tomlinson, "Applications of GRIN-rod lenses in optical fiber communication systems," *Appl. Opt.*, vol. 19, pp. 1127–1138, Apr. 1980.

[10] S. B. Sevastianov, S. M. Vatnik, and A. P. Mayorov, "Shaping of the end of a multimode optical fiber for efficient coupling light from a laser diode," *Appl. Opt.*, vol. 38, pp. 77–85, Jan. 1999.

[11] Y.-M. Jung, S.-U. Alam, and D. J. Richardson, "Compact few-mode fiber collimator and associated optical components for mode division multiplexed transmission," in *Proc. Opt. Fiber Commun. Conf.*, Anaheim, CA, USA, 2016, Paper no. W2A.40.

[12] P. Sillard, M. Astruc, D. Boivin, H. Maerten, and L. Provost, "Few-mode fiber for uncoupled mode-division multiplexing transmissions," in *Proc. 37th Eur. Conf. Expo. Opt. Commun.*, Geneva, Switzerland, 2011, Paper no. Tu.5.LeCervin.7.

[13] H.-M. Yang, S.-Y. Huang, C.-W. Lee, T.-S. Lay, and W.-H. Cheng, "High-coupling tapered hyperbolic fiber microlens and taper asymmetry effect," *J. Lightw. Technol.*, vol. 22, no. 5, pp. 1395–1401, May 2004.

[14] S. Yakunin and J. Heitz, "Microgrinding of lensed fibers by means of a scanning-probe microscope setup," *Appl. Opt.*, vol. 48, pp. 6172–6177, Nov. 2009.

[15] H. M. Presby, A. F. Benner, and C. A. Edwards, "Laser micromachining of efficient fiber microlenses," *Appl. Opt.*, vol. 29, pp. 2692–2695, Jun. 1990.

[16] F. Schiappelli *et al.*, "Efficient fiber-to-waveguide coupling by a lens on the end of the optical fiber fabricated by focused ion beam milling," *Microelectron. Eng.*, vol. 73/74, pp. 397–404, 2004.

[17] K. Shiraishi, N. Oyama, K. Matsumura, I. Ohishi, and S. Suga, "A fiber lens with a long working distance for integrated coupling between laser diodes and single-mode fibers," *J. Lightw. Technol.*, vol. 13, no. 8, pp. 1736–1744, Aug. 1995.

[18] K. Shiraishi *et al.*, "A novel lensed fiber with a focused spot diameter as small as the wavelength," in *Proc. Opt. Fiber Commun. Conf. Expo. Nat. Fiber Opt. Eng. Conf.*, Anaheim, CA, USA, 2007, Paper no. OWI2.

[19] M. Thual, P. Chanclou, O. Gautreau, L. Caledec, C. Guignard, and P. Besnard, "Appropriate micro-lens to improve coupling between laser diodes and singlemode fibres," *Electron. Lett.*, vol. 39, pp. 1504–1506, 2003.

He Wen received the B.E. and Ph.D. degrees in communication engineering from the Beijing University of Posts and Telecommunications, Beijing, China, in 2000 and 2005, respectively. From 2006 to 2008, he was a Postdoctoral Researcher with Tsinghua University, Beijing. From 2008 to 2014, he was a Lecturer and then an Associate Professor with Tsinghua University. Since 2014, he has been a Visiting Scholar with CREOL, University of Central Florida. He has authored and coauthored more than 90 journal and conference papers, and owned 8 patents. His current research interests include spatial-division multiplexing technologies in optical access networks, analog signal transmission and processing.

Huiyuan Liu, biography not available at the time of publication.

Yuanhang Zhang received the B.S. degree in information engineering from Tianjin University, Tianjin, China, in 2015, and he is currently working toward the Ph.D. degree at CREOL, University of Central Florida, Orlando, FL, USA. His research interests include integrated photonics, optoelectronics, and optical fiber communication.

Jian Zhao, biography not available at the time of publication.

Pierre Sillard (M'09) was born in Versailles, France. He received the Engineering Diploma from Telecom Paris Tech, Paris, France, in 1994, and the Ph.D. degree in optics from the University of Paris VI, Paris, in 1998, in collaboration with the Thales Research and Technology, Paris, on the subject of nonlinear interactions in laser resonators.

He has been working in the field of optical fibers since 1999, and he is currently with Prysmian Group, Haisnes, France. He has authored and coauthored more than 150 papers and holds more than 60 patents. His research interests include modeling and characterizing optical fibers and systems.

Dr. Sillard is a Member of the Optical Society of America. In 2004, he received the TR35 Innovator Award from *MIT Technology Review*. He serves as a Reviewer and Committee Member of several journals and conferences.

Rodrigo Amezcua Correa received the B.Eng. degree from the National Autonomous University of Mexico in 2002, and the Ph.D. degree from the Optoelectronics Research Centre, University of Southampton, in 2008.

He then joined the Centre for Photonics and Photonic Materials, Bath University, as a Postdoctoral Researcher in the field of fiber optics. In 2011, he joined the College of Optics and Photonics, University of Central Florida, as a Research Assistant Professor where his research focuses on fiber optics and fiber optics components.

Guifang Li (F'13) received the Ph.D. degree in electrical engineering from the University of Wisconsin at Madison. He is currently a Professor of optics, electrical and computer engineering and physics with the University of Central Florida. His research interests include optical communications and networking, RF photonics, all-optical signal processing, free-space optics and optical imaging.

Dr. Li is a Fellow of SPIE, the Optical Society of America, and the National Academy of Inventors. He served as a Deputy Editor for *Optics Express*, and an Associate Editor for *Optical Networks*, *Chinese Optics Letters*, and IEEE Photonics Technology Letters. He currently serves as the Overseas Associate Editor-in-Chief of *Frontiers of Optoelectronics*, and Associate Editors for OSA's *Optica* and the IEEE Photonics Journal. He is the recipient of the NSF CAREER award, and the Office of Naval Research Young Investigator Award.